Micron-Scale Friction and Sliding Wear of Polycrystalline Silicon Thin Structural Films in Ambient Air

Daan Hein Alsem, Michael T. Dugger, Eric A. Stach, and Robert O. Ritchie

***Abstract*—Micron-scale static friction and wear coefficients, surface roughness, and resulting wear debris have been studied for sliding wear in polycrystalline silicon in ambient air at micro-Newton normal loads using on-chip sidewall test specimens, fabricated with the Sandia SUMMiT V^{TM} process. With increasing number of wear cycles friction coefficients increased by a factor of two up to a steady-state regime, concomitant with a decay (after an initial sharp increase) in the wear coefficients and roughness. Wear coefficients were orders of magnitude smaller than reported macroscale values, suggesting that the wear resistance is higher at micrometer dimensions. Based on our observations, a sequence of micron-scale wear mechanisms is proposed involving: 1) a short *adhesive wear* regime ($< 10^4$ cycles), where the oxide is worn away and the first silicon debris particles form and 2) a regime dominated by *abrasive wear*, where silicon particles (50–100 nm) are created by fracture through the grains ($\sim$500 nm). These particles subsequently oxidize and agglomerate into larger debris clusters, while "ploughing" by this debris leads to abrasive grooves associated with local cracking events rather than plastic deformation. [2007-0292]**

***Index Terms*—Friction, microelectromechanical systems (MEMS), silicon, thin films, wear.**

I. Introduction

A WIDE RANGE of microelectromechanical systems (MEMS) are now found in consumer products and defense/space components; many of them containing thin silicon structural films. Examples are sensors (e.g., pressure, acceleration, gas), gyroscopes, inkjet printer heads, mirror arrays for projectors, optical switches (data transfer, weapon triggering), and microneedles (e.g., for drug delivery) [1]. These applications represent significant progress in miniaturization with the advantage of mass production, as MEMS components can be made using relatively inexpensive large-volume fabrication techniques.

Despite the increase in the application and use of MEMS, basic scientific studies on the underlying physical mechanisms responsible for different failure modes are fewer in number. This is unfortunate because identifying these mechanisms may be very important, since the large surface-to-volume ratio of micron-scale structures can change the magnitude of the relevant forces and as a result the salient failure modes and associated physical mechanisms [2], [3]. Moreover, although silicon is exceptionally strong ($\sim$4 GPa [4]–[6]), it is inherently brittle with a low fracture toughness ($K_{\mathrm{Ic}} \sim 1$ MPa$\sqrt{\mathrm{m}}$ [7], [8]), which markedly affects its performance as a structural material in MEMS devices.

Potential failure modes in silicon microsystems are adhesion [2], [9], fatigue [2], [6], [10]–[12], and wear [2]. Adhesion failures occur when free-standing MEMS components stick together, thereby impeding their motion. This can occur either during processing, specifically during the wet release and drying process step caused by a meniscus ("in-process stiction") or during operation when components touch and adhere. Although several different solutions for this issue have been proposed, including the procedure of critical-point drying after release and the application of hydrophobic and/or low surface energy coatings (e.g., [13]), this is still one of the major challenges with respect to MEMS reliability.

Fatigue, specifically very high-cycle fatigue, of silicon represents another potential failure mode for MEMS devices, which is particularly interesting as this phenomenon does not occur in silicon on the macroscale. However, at the micron scale, it has been associated with a mechanism involving moisture-assisted subcritical cracking within the stress-assisted thickened oxide layer; in thin films, this enables cracks to grow within the oxide layer to the critical size required for catastrophic failure of the entire microdevice [6], [10]–[12].

Wear of silicon micron-scale structures used in MEMS devices can also be an issue; however, from the perspective of the reliability of MEMS, approaches based on physical mechanisms have been limited by the fact that wear mechanisms in thin-film silicon are largely unknown. Early research on single-crystal silicon wafers, using pin-on-disk testing, resulted in a proposed set of wear mechanisms similar to those for bulk metals: namely abrasion, chipping and flattening of protrusions, plasticity, and delamination wear [14]–[17]. One of the

Manuscript received December 6, 2007; revised March 6, 2008. First published July 22, 2008; current version published October 1, 2008. This work was supported by the Director, Office of Science, Office of Basic Energy Sciences, Division of Materials Sciences and Engineering, U.S. Department of Energy, under Contract DE-AC02-05CH11231 at the Lawrence Berkeley National Laboratory (LBNL). Subject Editor M. Mehregany.

D. H. Alsem is with the Materials Sciences Division, Lawrence Berkeley National Laboratory, Berkeley, CA 94720 USA, and also with the National Center for Electron Microscopy, Lawrence Berkeley National Laboratory, Berkeley, CA 94720 USA.

M. T. Dugger is with the Materials Science and Engineering Center, Sandia National Laboratories, Albuquerque, NM 87185 USA.

E. A. Stach is with the School of Materials Engineering and Birck Nanotechnology Center, Purdue University, West Lafayette, IN 47907 USA.

R. O. Ritchie is with the Materials Sciences Division, Lawrence Berkeley National Laboratory, Berkeley, CA 94720 USA, and also with the Department of Materials Science and Engineering, University of California, Berkeley, CA 94720-1760 USA (e-mail: RORitchie@lbl.gov).

Digital Object Identifier 10.1109/JMEMS.2008.927751

1057-7157/$25.00 © 2008 IEEE

TABLE I
OVERVIEW OF SILICON STATIC COEFFICIENTS OF FRICTION DATA FROM SLIDING EXPERIMENTS AGAINST DIFFERENT MATERIALS AT DIFFERENT LENGTH SCALES (POLY IS POLYSILICON, SCS IS SINGLE CRYSTAL SILICON)

	Static Friction Coefficient		**Static Friction Coefficient**
Macro-Scale	range: 0.18-0.6	**Micro-Scale**	range: 0.25-1.1
Si / SiO_2	0.39 (vacuum) - 0.55 (air ~10^{-3}N) Pin on disc [21]	Poly / Poly	1.1 (~11 μN) Sandia sidewall-device [23]
Si / SiN_x	0.35 (vacuum) - 0.40 (air ~10^{-3}N) Pin on disc [21]	Poly / Poly	0.7 (up to 100 μN) SCREAM sidewall friction [24]
SCS / Al_2O_3	0.18 (0.1N) - 0.60 (1N) Ball on disc [22]	Poly / Poly	0.7 (~ 3 μN) Sidewall friction [25]
SiO_2 / SiO_2	0.2 (vacuum) - 0.43 (air ~10^{-3}N) Pin on disc [21]	Poly / Poly	0.25 to ~1 (~ 106 μN) Sandia nano-tractor [26]
		Poly / SCS	0.48 - 0.28 (5.3 - 113 μN) Micro-features on disc [27]
		Poly / SiO_2	0.85 - 0.70 (5.3 - 113 μN) Micro-features on disc [28]
		SCS/SCS	0.6 - 1 (~ 1 N) Pin on disc [28]
		SCS/SCS	0.9 (~75 μN) Rounded wedge on flat [29]

earliest on-chip MEMS microwear studies was performed by Mehregany *et al.* [18], [19] where the change in the gear ratio of an n^+-type polycrystalline silicon (polysilicon) MEMS wobble motor was indirectly used to determine wear. They observed that, initially, the gear ratio decreased relatively quickly before settling into a nominal steady-state mode, where it remained roughly constant (or even increased slightly). Early work on defining static friction coefficients[1] in silicon MEMS [20] suggested that values were high (on the order of five); however, more recent studies report more reasonable values ranging from 0.25 to 1.1 (normal loads typically in the micronewtons range, Table I). In comparison, corresponding macroscale friction coefficients are slightly lower (despite the scatter) at 0.18–0.6 (normal loads in the milli-Newtons to Newtons range, Table I).

Thin-film silicon friction and wear studies, by Ashurst *et al.* [13], [23], [30], [31], have focused on preventing wear by means of coatings, specifically by examining adhesion, stiction, friction coefficients, and the surface contact angles of several molecular thin organic coatings on silicon MEMS. These authors found that the coefficient of friction could be lowered by more than one order of magnitude by applying such coatings to polysilicon structures. Beerschwinger *et al.*'s study [32], [33] on microfabricated surfaces in a macroscale specimen-on-disk setup measured the surface roughness and wear volume for the wear of single crystal silicon, doped and undoped polysilicon. For single crystal silicon, these authors proposed a mechanism of asperity contact/wear followed by atomistic-scale wear, whereas for polysilicon they report morphological evidence of plasticity. They also implied that these governing mechanisms may be different at high and low contact loads as the wear rates at the high loads are so much larger. Atomic-force microscope scratch tests have also been used to determine tribological properties of different types of silicon thin films (e.g., [34], [35]); this approach, however, does not necessarily capture the same tribological interactions that are found in MEMS contact interfaces.

Despite these numerous studies on the tribology of thin-film silicon, which were recently reviewed in [36], the wear mechanisms themselves are rarely the focus of the individual research; consequently, there is currently no clear picture of what the prevailing mechanisms are that cause wear in thin-film silicon. However, there are some studies that do provide some detail on possible wear mechanisms. First, Tanner *et al.* [37], [38] proposed that an adhesive wear mechanism prevails, and that this is responsible for failure of polysilicon microengines. Specifically, during adhesive wear, asperities on two contacting surfaces adhere by plastic flow, resulting in the asperities cold-welding together; owing to continuing movement of these surfaces, fracture occurs away from the bonded interface leading to augmented asperities and wear debris. Alternatively, Patton *et al.* [39]–[41] have suggested two mechanisms: one for silicon wear *in vacuo* and the other in (dry) air. Due to the absence of moisture or oxygen *in vacuo*, the native oxide layer is presumed to wear off without being regenerated, thereby permitting Si–Si bonds to be formed between the two wearing surfaces, which in turn leads to asperity fracture or grain pull out. Conversely, in air, the oxide layer regenerates, resulting only in wear of silicon dioxide, created by surface reaction of silicon with oxygen in the air, with no direct wear at all of the silicon itself.

The lack of a clear mechanistic description of wear in thin-film silicon provides the rationale for this paper: to identify and characterize the principal mechanisms of micron-scale thin-film polysilicon wear in MEMS at micro-Newton normal loads. Specifically, our approach is to combine on-chip MEMS testing with atomic force and electron microscopy to examine wear debris and worn surfaces, together with quantitative measurements of the wear volume, surface roughness,

[1]The (static) friction coefficient is the ratio of the frictional forces to the normal forces between two surfaces.

and static friction coefficients as function of the number of cycles worn, in order to provide an underlying basis for the mechanisms that control wear in polysilicon at micrometer dimensions; further we compare this behavior with macroscale results. Previously, we have investigated wear debris by analytical transmission electron microscopy (TEM) [42]. These observations and the work presented here are used to suggest a sequence of micron-scale wear mechanisms involving: 1) a short adhesive wear regime, where the silicon oxide is worn away and the first silicon debris particles form, and 2) a regime dominated by abrasive wear, where silicon particles are created by fracture through the grains. These particles subsequently oxidize and agglomerate into larger debris clusters, while "ploughing" by this debris leads to abrasive grooves associated with local cracking events rather than plastic deformation.

II. Experimental Methods

On-chip n^+-type polysilicon MEMS sidewall friction/wear test specimens were used to study wear and friction; these were fabricated with a perflurordecyltrichlorosilane, $CF_3(CF_2)_7(CH_2)_2SiCl_3$ (FDTS), monolayer coating on the polysilicon[2] using the Sandia National Laboratories SUMMiT V^{TM} process (Fig. 1) [43].[3] Specifically, the device consists of two electrostatic comb drive actuators that create motion in two orthogonal directions. The electrostatic actuation is based on applying a bias a cross the set of combs in the comb drive, with the magnitude of the force created given by

$$F = \varepsilon \frac{nh}{g} V^2 \tag{1}$$

where ε is the dielectric constant of the medium between the comb finger, n is the number of comb fingers, h is the thickness of the comb fingers, g is the gap between the fingers, and V is the applied voltage [23], [44]. Applying a dc voltage to one of the actuators pulls the beam against a post; sinusoidal ac signals leading to the other (perpendicular) comb drive then cause the beam to slide back and forth against the post (Fig. 1).[4]

To determine the average normal force between the beam and the post during the wear process, the devices were first calibrated by noting the applied dc voltage in the normal comb drive and the bending of the beam up to when it (almost) touches the post; using elastic beam bending theory and (1), the normal force can be determined as function of the applied voltage to the normal comb drive. The same devices can also be used to determine the static coefficients of friction μ; this is achieved by applying a normal load by means of a normal dc voltage and increasing the tangential force by ramping a second

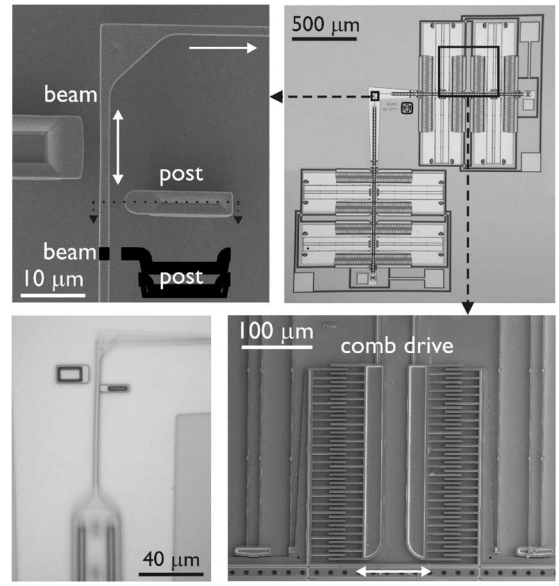

Fig. 1. On-chip n^+-type polysilicon sidewall friction/wear test device. The device produces two-axis motion provided by electrostatic comb drives used to pull a beam against a post and wearing the two surfaces (the contact cross section is superposed onto the upper left image). The bottom left image shows the device in motion during a wear test.

dc voltage signal (~1 V/s) and noting the voltage where the beam first slips along the post (as observed through a 1000 × optical microscope). A (calibrated) force balance of the beam touching the post is used to obtain the value for the static coefficient of friction. Note that because the force calibration is conducted when the beam and the post are not in contact and the calibration curve does not show a change of slope as the beam approaches the post, these values of the static coefficient of friction do not include an additional adhesive force component caused by the close proximity of the beam and post surfaces. More details on the calculations of the static coefficient of friction and the force calibration procedure can be found in Ashurst *et al.* [23].

All devices were operated in ambient air (25%–50% relative humidity, 23 °C–27 °C) under normal contact loads of 3–6 μN at 100 Hz[5] with peak-to-peak sliding amplitudes of 4–8 μm per cycle, while some of the devices that were used for electron microscopy debris characterization were partially run at 200 and 400 Hz. The number of wear cycles ranged from below 100 to almost 2 million, giving total sliding distances of up to 20 m. Scanning electron microscopy (SEM) images of worn surfaces and the associated wear debris were used to determine the morphology of the worn areas. The SEM imaging was performed using a JEOL 6340F Field Emission SEM or an FEI Strata DB235 Dual-Beam Focused Ion Beam (FIB). The latter was also used for the atomic-force microscopy (AFM) sample preparation. FIB TEM sample preparation techniques [42], [46] followed by TEM observations, utilizing a 300-kV JEOL 3010 (LaB_6 filament), were used to acquire more detailed information on the wear debris and worn surfaces.

[2]The coating was applied for ease of transport and handling and released via the following steps in solution at room temperature: release etched (buffered HF), rinsed with deionized (DI) water, oxidized with H_2O_2, rinsed with DI water, transferred to isopropyl alcohol and then to isooctane, transferred to 1-mM solution of the monolayer in isooctane and held in solution for 2 h, transferred to neat isooctane, then to isopropyl alcohol and to DI water, before finally being removed from DI water and air dried on class ten clean bench.

[3]More information on the SUMMiT V^{TM} process at http://mems.sandia.gov.

[4]Note that during the wear tests, the beam and post are not perfectly aligned (as schematically suggested in Fig. 1), and the beam is elevated somewhat with respect to the post due to comb-drive levitation effects [45].

[5]This frequency was chosen to allow accumulation of large numbers of cycles, as well as accurate number of wear cycle measuring in the initial stages of friction/wear. Effects of frequency have not been included in this paper, but have been described elsewhere [37].

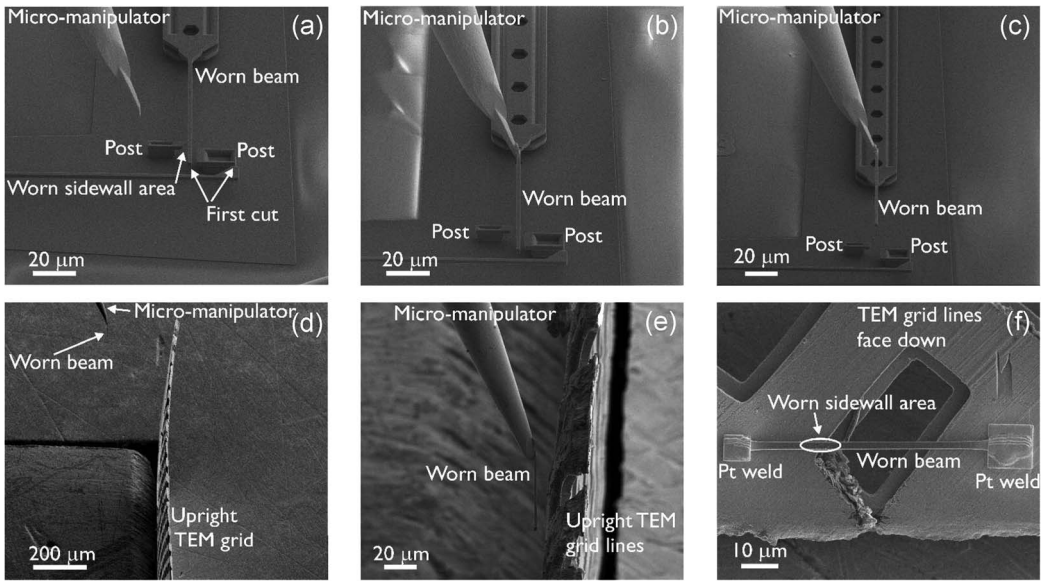

Fig. 2. Lift-off AFM sample preparation, using a dual-beam FIB mounted with a tungsten micro-manipulator. (a) and (b) Worn beam is cut from the device while platinum-welded to the manipulator (the first cut is done before welding, the second after) and (c) lifted off the chip. (d) and (e) Sample is transported to a semicircular TEM specimen grid (half of a standard 3-mm circular copper grid) and is welded to the upright (vertical) grid. (f) Sample attached to TEM grid after rotating the grid 90° (horizontal) and securing the welds to the grid; the worn side (initially a sidewall) now faces up.

AFM of worn surfaces was performed by using an Asylum Research MFP-3D in noncontact mode to acquire root mean square (rms) surface roughness before and after wearing of the sidewalls, as well as to measure the volume of material worn away in the polysilicon devices. Single crystal silicon AFM tips were used during imaging with an estimated tip radius less than 7 nm. SEM measurements showed the tip radius to be approximately doubled after one full day of imaging. The AFM samples were prepared using FIB sample preparation techniques similar to that for TEM [42], [46]; a worn beam of the sidewall device was cut out of the device and moved to (half a) copper TEM sample grid (Fig. 2) by means of a sharp tungsten micromanipulation needle (Omniprobe), to which the beam was welded (temporarily—during transport) using platinum [Fig. 2(a)–(e)]. For AFM imaging, the worn sidewall surface of the beam needed to face upwards, so the TEM grid was vertically positioned when the beam was attached to it. The final AFM sample consisted of a silicon beam attached to a fine TEM grid spanning two grid lines with the worn surface facing upwards when the grid is horizontally positioned [Fig. 2(e) and (f)].

III. Results

A. Friction Coefficients

The polysilicon test devices (Fig. 1) were first used to investigate friction. Specifically, static friction coefficients were measured in ambient air at different points during the wear process. Friction data, where every data point consists of the average and standard deviation of five to ten friction coefficient measurements, show an initial static friction coefficient of 0.12 ± 0.02 (an example with a normal load of 4.8 μN and amplitude of 5.7 μm per cycle is shown in Fig. 3). After ~150 000 wear cycles, the friction coefficient had increased by a factor of two and reached a constant steady-state value of 0.24 ± 0.07 (0.17 and 0.28 in Figs. 3 and 4, respectively).

To gain insight into how the friction coefficient is affected by the morphology of the wearing surface and the prevailing wear mechanisms, the worn surface of the device was imaged using SEM after acquiring each measured value of the friction coefficient. The resulting friction data (Fig. 4, where the normal load is 5.2 μN and sliding amplitude 5.8 μm per cycle) show similar trends to Fig. 3; with increasing wear cycles, the static friction coefficient increases from an initial value (~0.13 in this example) to a steady-state value (with fluctuations) approximately twice as large (~0.28). Corresponding SEM images of the wearing surface (Fig. 4) indicated that abrasive wear grooves form early in the wear process (at $< 27\,000$ cycles), well before the steady-state value of the static coefficient of friction is reached. These wear grooves become larger and more numerous with increasing number of wear cycles. The development of the static coefficient of friction in the early stages of the wear process is shown in Fig. 5 (normal load 5.4 μN, sliding amplitude 8.0 μm per cycle), where it remains constant (~0.11) over the first 4000 cycles, before rising to a higher steady-state value. The SEM image of the worn surface at 4000 cycles show that there is some wear debris generated before the first abrasive grooves appear at 8000 cycles (the oval marks in Fig. 5 delineate the first abrasive grooves); this implies that a different wear mechanism (most likely adhesive wear) is active before the abrasive wear regime begins.

Note that the friction coefficient is not fully independent of the normal contact load; control measurements at contact loads between 3 and 9 μN revealed a trend of slightly higher friction coefficients with higher pressure, consistent with previous studies [39], [40]. Specifically, lowering the normal contact force by a factor of three reduces the friction coefficient on average by ~10% (values range from +10% to –30%). Given the fluctuation in the measured friction coefficients, this small variation was deemed not to be significant for the range of contact loads used in this paper (3–6 μN).

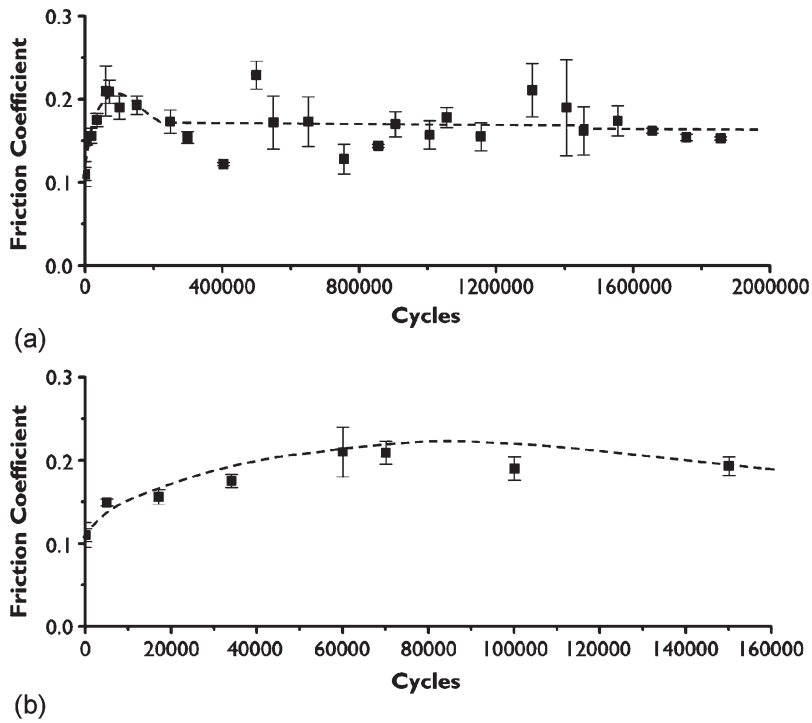

Fig. 3. Static coefficients of friction after different numbers of wear cycles (normal contact load: 4.8 μN, cyclic amplitude 5.7 μm per cycle). In (a), the graph shows the general trend, whereas in (b), the graph shows the first 160 000 cycles from the same experiment. After an initial increase in the first $\sim$150 000 cycles, the friction coefficient fluctuates around a steady-state value.

B. Micron-Scale Wear Coefficients and Roughness

After FIB sample preparation (Fig. 2), AFM topographic scans were performed on the worn areas of several sidewall devices. A typical example of a topographical map of a worn area (Fig. 6) yields 3-D information on both the rms sidewall roughness as well as the volume of worn material. The example in Fig. 6 clearly shows a deep abrasive wear groove with wear debris scattered around this groove. By examining the shape and depth of these grooves by AFM and using both AFM and SEM measurements of the width and length of the wear grooves, the volume of worn (removed) material was calculated. Such information was used to compute the dimensionless wear coefficients, k, *at the micron-scale*, based on Archard's law [47], [48], a phenomenological relationship describing the mechanical wear of materials, viz.,

$$V_{\mathrm{w}} = k\frac{SP}{3H} \tag{2}$$

where V_{w} is the worn volume (in cubic meters), S is the total sliding length (in meters), P is the normal load between the surfaces (in Newtons), and H is the material hardness (in pascal) (11.5 GPa for n^+-type polysilicon films [34]). The micron-scale wear coefficient k represents the wear resistance of a material, specifically the probability that a local contact junction between two surfaces forms a wear particle. Measured depths of abrasive wear grooves were typically 20–60 nm. Sources of error in the worn volume arise from 1) the finite radius of the AFM tip (particularly at small depth readings and high depth/width aspect ratio grooves) and 2) the wear of the post; however, the latter was significantly smaller (10%–20% of the total wear, as estimated from SEM images) than the wear of the beam. The latter effect is most likely caused by the fact that the width of contact on the post is smaller than the grain size, and therefore, the post can effectively be considered single crystal silicon, which is harder than polycrystalline [34], [35], whereas the sliding length on the beam contains multiple grain boundaries, which can act as stress concentrators. These effects are included in the error bars for the wear coefficients in Fig. 7.

Results for wear coefficients calculated from different devices as a function of the number of wear cycles are shown in Fig. 7 and indicate that after an initial rise to $k = 1.1 \times 10^{-4}$, the coefficients progressively decay to a value of $k = 8.8 \times 10^{-6}$ as the accumulated wear cycle count increases. To relate these results to the surface morphology, rms sidewall roughnesses were measured (in several $\sim$4 $\mu\mathrm{m}^2$ areas along the worn section of the beam) at increasing numbers of wear cycles using the same devices used for the data points in Fig. 7, as shown in Fig. 8. Unworn specimens had an rms roughness of 10 ± 2 nm; these values are similar to reported measurements on polysilicon from the same fabrication source [49]. After an initial steep increase, the surface roughness can be seen to reach a maximum of $\sim$42 nm before 5×10^5 wear cycles, before decaying to half that value (21 nm) over the next 1.5×10^6 cycles.

C. Debris and Surface Characterization

In previously published work by Alsem *et al.* [42], more detailed information on the creation of wear particles was obtained using SEM and TEM of the wear debris and worn surface after hundreds of thousands to millions of cycles. These

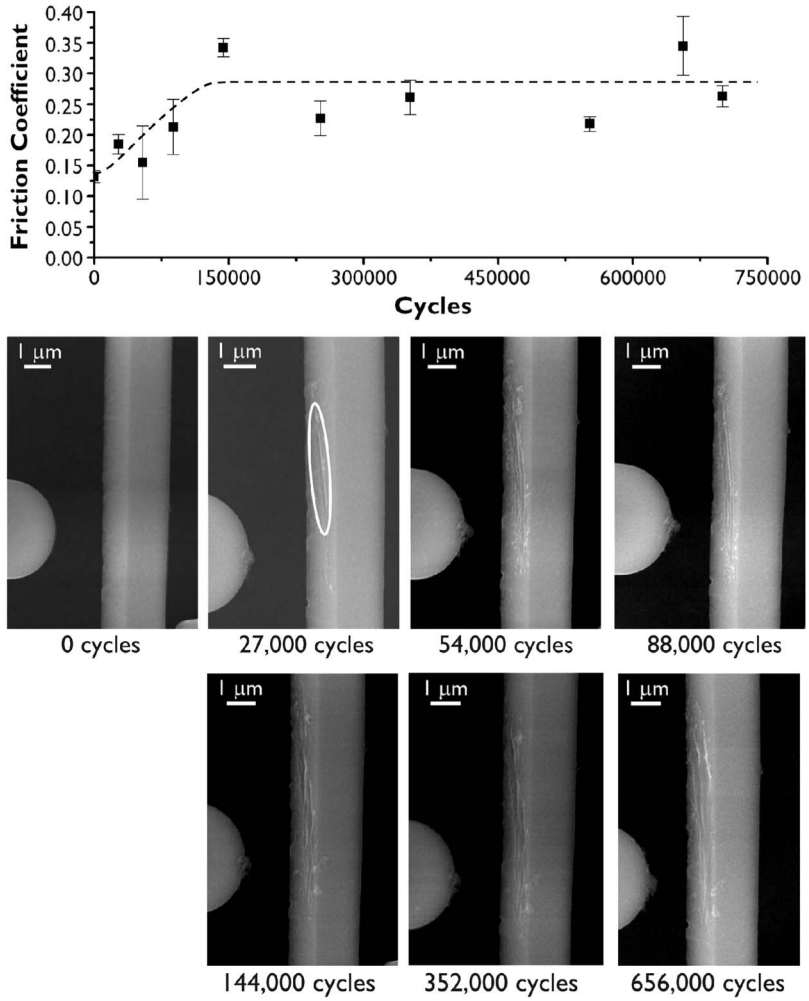

Fig. 4. SEM silicon wear device surface morphology images during a wear experiment (normal contact load: 5.2 μN, cyclic amplitude 5.8 μm per cycle), showing the development of abrasive grooves in a very early stage of the wear experiment (before 27 000 cycles as marked by a white oval), which continue to increase in number as the wear process continues. Images were taken at 20-kV acceleration voltage at 30° sample tilt.

studies found the size of the abrasive wear grooves to be several micrometers in length and ~100–400 nm wide [Fig. 9(a) and (b)] and roughly revealed spherical debris particles ranging in diameter from ~50 to 500 nm (Fig. 9(a), (b), and (d) [42]). The larger debris particles consisted of agglomerates made up from smaller particles, sized 50–100 nm, with an amorphous structure, as shown by TEM selected area diffraction (SAD) patterns in Fig. 9(d) [42]. Comparison of these diffraction patterns to reference patterns of silica and amorphous silicon (e.g., [50], [51]) indicated that both amorphous materials can yield similar diffraction patterns; consequently, SAD patterns cannot provide a conclusive determination of the chemical nature of the wear debris. Calibrated TEM x-ray dispersive spectroscopy (EDS), however, showed that the debris particles have a 1 : 2 Si:O ratio on the edge of the particle, but a 1 : 1 Si:O ratio in the center [42], suggesting the outer shell consists of stochiometric SiO_2, whereas the particle core could be a mix of SiO_2 and amorphous Si or SiO_x (x ~ 1) silicon oxide.

FIB-sectioned TEM cross-sectional specimens of worn regions indicate that the grain size of the (unworn) silicon is about 450 nm [52]. No evidence of dislocation pileups could be seen below or in the surface layers (Fig. 9(c) [42]). A graphical summary of the different length-scales (on a logarithmic scale) of the different features of the worn surfaces and wear debris formed during micron-scale wear of thin-film silicon is shown in Fig. 9(a).

IV. Discussion

In this study of friction and wear of polysilicon thin films, the evolution of the micrometer-scale friction coefficients, wear coefficients, and rms roughness, as well as surface morphology, has been measured as a function of the number of worn cycles. These results are now compared with known macroscale trends and values and are used to derive detailed micron-scale wear mechanisms for polysilicon in ambient air.

First, with respect to static coefficients of friction: comparing previously published values of static friction coefficients on the micron-scale with values from macroscale experiments (Table I), indicates that the steady-state friction coefficient values of 0.24 ± 0.07 measured in this paper (Figs. 3–5) fall within the lower range of the published micron-scale friction coefficients (Table I), yet are similar to typical friction coefficients for silicon reported in macroscale studies. Indeed, the

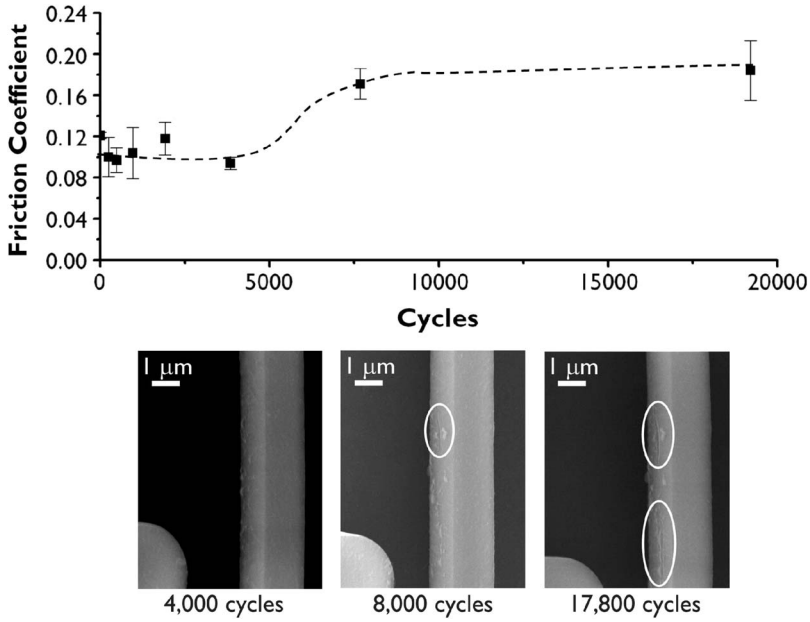

Fig. 5. Friction coefficient data and SEM images of worn surfaces during the first 20 000 wear cycles (normal contact load: 5.4 μN, sliding amplitude 8.0 μm per cycle). The first abrasive groove can be seen after 8000 cycles, whereas there is also significant wear debris that is not associated with "ploughing" grooves before that (4000 cycles), indicating that another (adhesive) wear regime is active before abrasion commences. Wear grooves on the worn surfaces are indicated by the white ovals. The images were taken at 20-kV acceleration voltage at 30° sample tilt.

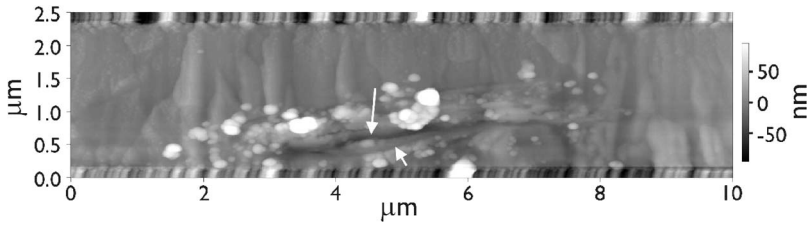

Fig. 6. AFM image of a worn region showing wear grooves (one major, marked with a large arrow and some smaller subgrooves, one of which is marked with a small arrow) after wear for 42 200 cycles at 5.4 μN. Outside the groove, both debris particles (bright features) and the columnar grain structure of the film (vertical oriented contrast across the height of the film) can be seen. Note the horizontal edges of the beam on the upper and lower end of the image that cause imaging artifacts (these areas have not been included in any of the quantitative measurements).

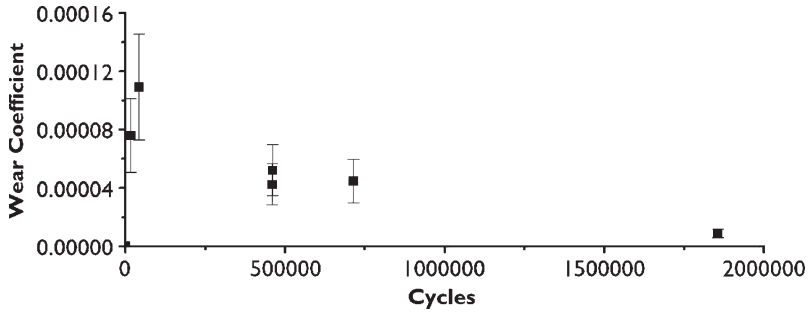

Fig. 7. Variation in the wear coefficient for polysilicon showing an initial rapid increase followed by a steady decrease with increasing number of wear cycles (normal contact loads $P = 3$–6 μN, cyclic sliding amplitude 4–8 μm, total sliding lengths $S \sim 0.3$–20 m).

starting value of the friction coefficient in this paper ($\mu \sim 0.12$) corresponds to the value for other polysilicon devices covered with an FDTS coating [53].

In addition to the quantitative values, the trends found in the evolution of the friction coefficient (Figs. 3 and 4) are qualitatively quite similar to macroscale measurements for metallic materials, where after an initial rise the friction coefficient approaches a steady-state value. In metallic materials, this is often caused by abrasion between surface asperities, which leads to an initial increase in friction before an equilibrium is reached between wear particle generation and the fracture/deformation of surface asperities and existing wear particles in the steady-state friction regime [54], [55]. However, for the micron-scale polysilicon friction investigated here, there were certain distinct differences involving the specific wear mechanisms in the early stages of the friction/wear process, and the large fluctuations of the steady-state friction coefficient once a nominal steady-state condition was reached. The evolution of the wear mechanisms

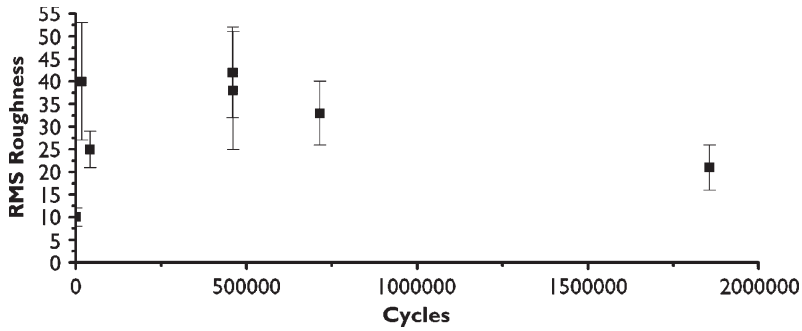

Fig. 8. RMS roughness as function of the number of wear cycles (normal contact loads 3–6 μN, cyclic sliding amplitude 4–8 μm) showing an initial sharp increase followed by a slow decrease as the number of wear cycles increases.

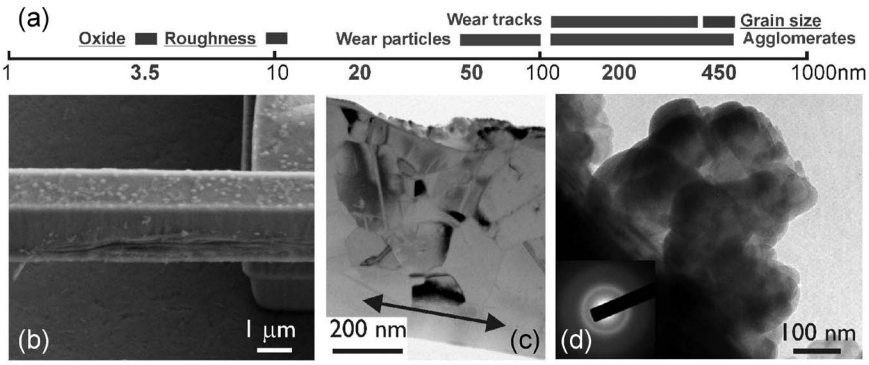

Fig. 9. (a) Logarithmic overview of the length scales of the different features found in worn polysilicon sidewall friction devices. The underlined features are the feature sizes that are determined by device processing parameters. (b) SEM micrograph of worn surface taken at 5 kV. (c) TEM cross section showing the grain structure and the lack of subsurface dislocations after the wear process. The wear direction is indicated by the arrow and the beam was worn on the top of the image (d). Typical TEM bright-field image and diffraction pattern of debris particle agglomerates show the particles to be amorphous and ~100–500 nm in size (after [42]).

in the early stages of wear can be deduced from the static friction coefficients (Fig. 3) as well as from the SEM images taken at different stages of the wear process (Figs. 4 and 5). During the first 4000 cycles, where the friction coefficient remains at $\sim 0.12 \pm 0.02$, the FDTS monolayer coating, which is typically ~2 nm thick [56], wears off by a molecular/atomistic adhesive wear mechanism; this is followed by an increase in friction coefficient as first the thin silicon oxide (~3.5 nm thick [11], [52]) is removed from the surface after which direct wear of the polysilicon commences. Because the monolayer and silicon oxide are so thin, they do not significantly contribute to the measured wear volumes. After the wear and removal of these thin surface layers, a short adhesive silicon wear regime dominates for several thousand cycles until a critical mass of particles is reached, at which time abrasive wear commences. This can be deduced from Fig. 5 where significant wear debris is visible at 4000 cycles before the first wear groove is observed after 8000 cycles. This sequence of micron-scale wear events is distinct from that of classical macroscale mechanisms where large surface asperities cause abrasion to commence from the first wear cycles [54].

Another difference between classical macroscale friction theory [54], [55] and the micron-scale experiments presented in this paper is the large scatter around the average steady-state friction coefficient shown in Figs. 3 and 4 (>150 000 cycles). Since the dominant wear mechanism remains the same after it reaches the steady-state friction value (Fig. 4), the fluctuations in friction found here are most likely due to local variations in the surface morphology. In particular, the real area of contact between the silicon surfaces can markedly change on a local scale after wear commences, which in turn affects the friction coefficient. This change in real area of contact can be caused by an alteration of the surface itself, or the changing presence of loose debris particles between the two wearing surfaces. Since the apparent contact area between the post and beam is of the order of 0.2 μm^2, the average minimum contact stress (with a load of 5 μN) is only about 25 MPa. As the stress needed to facilitate cracking in polysilicon is orders of magnitude higher than this value, this indicates that the contact stresses in this system during operation are determined by the real area of contact (as well as the friction force). The real area of contact in turn is controlled by variations in the local surface morphology (i.e., the local roughness). Note that such local variations in roughness would not appear in the rms roughness measurements shown in Fig. 8, because the apparent contact area (which is larger than the real contact area) is smaller than the sample region (~ 4 μm^2) used to acquire the rms roughness data. This suggests that it is the local contact morphology that controls the scatter in the value of the coefficient of friction in the steady-state regime.

A striking difference between macroscale tests and the micron-scale tests presented here is the magnitude and evolution of the wear coefficients (Fig. 8). Depending on the wear conditions, macroscale wear coefficients for polysilicon

on polysilicon in ambient air (measured at normal loads of 0.15–0.49 N) are reported to be 10^{-14} to 10^{-12} $\mathrm{m}^3/\mathrm{N}\cdot\mathrm{m}$ [57], [58]; corresponding dimensionless wear coefficients [as computed using Archard's law: (2)] vary between 3.45×10^{-2} to 3.45×10^{-4}. In stark contrast, values of the wear coefficients measured in this paper (Fig. 8) at the microscale are orders of magnitude smaller, with dimensionless wear coefficients varying between 10^{-4} to $< 10^{-5}$. Also, general experimental trends show abrasive wear to yield wear coefficients of 10^{-1} to 10^{-4} [55], as compared to the values found in this paper which were not only less than earlier reported macroscale silicon experiments, but also less than other macroscale abrasive wear experiments. This means that the wear resistance increases as the size-scale of the wear process is reduced to the micron-scale, implying that at the lower normal loads associated with micron-scale wear, there is a decrease in the probability of creating wear particles. This could be caused by the fact that the strength and fracture properties of silicon can be different at small dimensions. Specifically, as the wear debris is of a size comparable with, or smaller than, the microstructural features in the silicon, this could lead to an apparent strengthening effect in the small volumes where the wear particles form, e.g., debris particles are smaller than the grain size, resulting in the reduction of the effect of grain-boundary cusps as stress concentrators and preferential crack initiation sites. Additionally, small micron-scale structures in silicon would statistically demonstrate higher fracture strength than macroscale structures. This effect essentially results from the fact that in a brittle material, the strength and fracture resistance, which in silicon control the generation of wear particles, are dependent on the existence of preexisting defects, and the probability of encountering such defects is diminished as the sampling volume is decreased. In addition to this increased wear resistance, the overall trend of a decreasing value in the micron-scale wear coefficient as the wear process progresses (Fig. 8), which parallels a similar trend seen in the values of the roughness (Fig. 7), is different to that of classical (macroscale) wear theory, which shows a constant wear coefficient during the wear process [55]. The measured decrease in wear coefficient suggests that after the initial creation of wear particles, they are slowly worn down as the wear continues and the probability of the creation of new debris particles decreases. In classical wear theory, this decreasing wear rate is generally not found.

TEM studies in this paper indicate that the scale of the wear debris is of similar order as the width of the wear grooves (Fig. 9); accordingly, we conclude that a primary mechanism of wear in micron-scale polysilicon at micro-Newton normal loads involves abrasive wear by wear particles which create "ploughing" grooves on the worn surface via fracture through the grains. Since this occurs during the early stages of wear (Figs. 4 and 5) and continues as the number of worn cycles increases, abrasive wear is clearly the dominant mechanism throughout most of the wear process. In terms of size scales (Fig. 9), the ~50–100 nm wear particles that are formed are smaller than the ~450 nm silicon grain size, but both are significantly larger than the roughness of the wearing surfaces (~12 nm). The wear debris particles oxidize heavily and amorphize during the wear process (after they are removed from the surface, aided by high contact stresses), evolving into particles with a SiO_2 outer layer and a SiO_x or (amorphous) Si core (as determined by EDS [42]). Such oxidation, coupled with the factor of roughly two difference in the molar volume of Si (12 $\mathrm{cm}^3/\mathrm{mol}$) and SiO_2 (27 $\mathrm{cm}^3/\mathrm{mol}$), means that these particles have a size of down to ~25–50 nm when they are removed from the surface and are thus created by fracture inside the grains.

Finally, it should be noted here that the processes that create wear debris appear to be controlled not by plastic deformation, but by fracture of the silicon, as there was absolutely no evidence of plasticity in the TEM cross sections of worn areas [42]. This is to be expected as dislocation plasticity in (unconstrained) silicon is invariably associated with temperatures above ~500 °C [59], and no such temperatures have been detected, even locally, in this system [42]. In general, there has been no direct evidence to date (e.g., from TEM imaging) where dislocations have been seen at arrested crack tips in silicon; room-temperature dislocation plasticity in silicon has only been observed to date during the high combined compressive and shear loads of a nanoindentation test [60]. Additionally, surface fatigue (delamination wear) can be ruled out because subcritical (subsurface) cracking does not occur in silicon and the time/cycle-dependent fatigue effects that have been seen in micron-scale silicon films are associated with subcritical cracking in silicon oxide on the surface [6], [10]–[12]. Indeed, neither subcritical cracks nor subsurface oxides were found in the cross-sectional TEM specimens [42]. Additionally, the measured wear coefficients decrease with increasing number of wear cycles (Fig. 9), whereas if a surface fatigue mechanism was operative, an opposite trend would be expected.

V. Summary and Conclusion

On-chip polysilicon sidewall friction/wear test specimens have been used to study friction, wear coefficients and wear mechanisms in sliding wear of polysilicon under micro-Newton loads at micron-scale dimensions with normal loads of 3–6 μN in ambient air. Measurements of the coefficient of static friction as the wear process progresses were correlated with SEM images of worn surfaces. Furthermore, devices worn to different numbers of cycles (cyclic amplitudes: 4–8 μm) were investigated using AFM in order to determine the rms surface roughness and corresponding evolution of the wear coefficient. Finally, wear debris and wearing surfaces were examined using high-resolution (transmission) electron microscopy, EDS, and the dimensions of the different features encountered used to conclude how the wear particles were formed. Micron-scale wear coefficients for silicon were found to be approximately one to three orders of magnitude smaller than have been reported in macroscale experiments, showing a relatively larger wear resistance at these smaller scales, most likely caused by the fact that the wear debris is of similar size or smaller than the microstructural features of the polysilicon and by the lower probability of fracture associated with smaller structural volumes due to their statistically smaller number of defects.

We conclude that the sliding wear of micron-scale silicon on silicon under micro-Newton normal loads (3–6 μN) occurs by the following mechanistic sequence.

1) An initial *adhesive wear regime* where first the FDTS monolayer coating and then the silicon oxide wears away during the first 4000 wear cycles. The removal of these layers creates freshly exposed silicon surfaces, which can come into contact to form strong covalent bonds. The wear mechanism then comprises adhesive wear of the silicon itself, during which the friction coefficient slowly increases, involving the creation of adhesive wear debris by fracture of the surface silicon grains.
2) As soon as a critical mass of wear particles has been generated (at less than 8000 cycles), the governing wear mechanism transitions from adhesive to (third body) abrasive wear (prior to when the steady-state value of the friction coefficient is reached). In this abrasive regime, wear grooves are created on the surface by the removal of more debris particles (50–100 nm with agglomerates up to ~500 nm) resulting from fracture through the grains (~450 nm). Such wear debris particles oxidize heavily and amorphize, such that they evolve into particles with a silica outer layer and a SiO_x or amorphous Si core. All of these processes are controlled by fracture and not by plastic deformation of the silicon, since no evidence of plasticity was found in TEM cross-sectional specimens.

ACKNOWLEDGMENT

The authors would like to extend thanks for the use of the Molecular Foundry, and, specifically the assistance of Dr. P. Ashby and Dr. F. Ogletree with the AFM training, and the National Center for Electron Microscopy, both operated at Lawrence Berkeley National Laboratory with the support of the U.S. Department of Energy under Contract DE-AC02-05CH11231. The authors would also like to thank the support from Sandia National Laboratories. Sandia is a multiprogram laboratory operated by Sandia Corporation, a Lockheed–Martin Company, for the U.S. Department of Energy's National Nuclear Security Administration under Contract DE-AC04-94AL85000.

REFERENCES

[1] N. Maluf and K. Williams, *An Introduction to Microelectromechanical Systems Engineering*. Norwood, MA: Artech House, 2004.
[2] A. D. Romig, Jr., M. T. Dugger, and P. J. McWhorter, "Materials issues in microelectromechanical devices: Science, engineering, manufacturability and reliability," *Acta. Mater.*, vol. 51, no. 19, pp. 5837–5866, Nov. 2003.
[3] K. Komvopoulos, "Surface engineering and microtribology for microelectromechanical systems," *Wear*, vol. 200, no. 1, pp. 305–327, Dec. 1996.
[4] T. Ando, M. Shikida, and K. Sato, "Tensile-mode fatigue testing of silicon films as structural materials for MEMS," *Sens. Actuators A, Phys.*, vol. 93, no. 1, pp. 70–75, Aug. 2001.
[5] H. Kapels, R. Aigner, and J. Binder, "Fracture strength and fatigue of polysilicon determined by a novel thermal actuator," *IEEE Trans. Electron Devices*, vol. 47, no. 7, pp. 1522–1528, Jul. 2000.
[6] D. H. Alsem, C. L. Muhlstein, E. A. Stach, and R. O. Ritchie, "Further considerations on the high-cycle fatigue of micron-scale polycrystalline silicon," *Scr. Mater.*, 2008, in press. doi.org/10.1016/j.scriptamat.2008.03.043.
[7] H. Kahn, N. Tayebi, R. Ballarini, R. L. Mullen, and A. H. Heuer, "Fracture toughness of polysilicon MEMS devices," *Sens. Actuators A, Phys.*, vol. 82, no. 1, pp. 274–280, May 2000.
[8] R. Ballarini, R. L. Mullen, Y. Yin, H. Kahn, S. Stemmer, and A. H. Heuer, "The fracture toughness of polysilicon microdevices: A first report," *J. Mater. Res.*, vol. 12, no. 4, p. 915, Apr. 1997.
[9] R. Maboudian, W. R. Ashurst, and C. Carraro, "Tribological challenges in micromechanical systems," *Tribol. Lett.*, vol. 12, no. 2, pp. 95–100, Feb. 2002.
[10] C. L. Muhlstein, E. A. Stach, and R. O. Ritchie, "A reaction-layer mechanism for the delayed failure of micron-scale polycrystalline silicon structural films subjected to high-cycle fatigue loading," *Acta Mater.*, vol. 50, no. 14, pp. 3579–3595, Aug. 2002.
[11] D. H. Alsem, R. Timmerman, B. L. Boyce, E. A. Stach, J. Th. M. De Hosson, and R. O. Ritchie, "Very high-cycle fatigue failure in micron-scale polycrystalline silicon films: Effects of environment and surface oxide thickness," *J. Appl. Phys.*, vol. 101, no. 1, p. 0137 515, Jan. 2007.
[12] D. H. Alsem, O. N. Pierron, E. A. Stach, C. L. Muhlstein, and R. O. Ritchie, "Mechanisms for fatigue of micron-scale silicon structural films," *Adv. Eng. Mater.*, vol. 9, no. 1/2, pp. 15–30, 2007.
[13] M. P. de Boer, D. L. Luck, W. R. Ashurst, R. Maboudian, A. D. Corwin, J. A. Walraven, and J. M. Redmond, "High-performance surface-micromachined inchworm actuator," *J. Microelectromech. Syst.*, vol. 13, no. 1, pp. 63–74, Feb. 2004.
[14] R. G. Bayer, "Influence of oxygen on the wear of silicon," *Wear*, vol. 69, no. 2, pp. 235–239, Jun. 1981.
[15] S. Danyluk and R. Reaves, "Influence of fluids on the abrasion of silicon by diamond," *Wear*, vol. 77, no. 1, pp. 81–87, Mar. 1982.
[16] S. Danyluk and J. L. Clark, "The wear rate of N-type Si (100)," *Wear*, vol. 103, no. 2, pp. 149–159, May 1985.
[17] D. E. Kim and N. P. Suh, "On microscopic mechanisms of friction and wear," *Wear*, vol. 149, no. 1/2, pp. 199–208, Sep. 1991.
[18] M. Mehregany, S. D. Senturia, and J. H. Lang, "Friction and wear in microfabricated harmonic side-drive motors," in *IEEE Solid-State Sens. Actuator Workshop Tech. Dig.*, 1990, pp. 17–22.
[19] M. Mehregany, S. D. Senturia, and J. H. Lang, "Measurement of wear in polysilicon micromotors," *IEEE Trans. Electron Devices*, vol. 39, no. 5, pp. 1136–1143, May 1992.
[20] M. G. Lim, J. C. Chang, D. P. Schultz, R. T. Howe, and R. M. White, "Polysilicon microstructures to characterize static friction," in *Proc. IEEE MEMS*, 1990, pp. 82–88.
[21] K. Deng and W. H. Ko, "A study of static friction between silicon and silicon compounds," *J. Micromech. Microeng.*, vol. 2, no. 1, p. 14, Mar. 1992.
[22] B. Bhushan and A. V. Kulkarni, "Effect of normal load on microscale friction measurements," *Thin Solid Films*, vol. 278, no. 1/2, p. 49, May 1996.
[23] W. R. Ashurst, C. Yau, C. Carraro, R. Maboudian, and M. T. Dugger, "Dichlorodimethylsilane as an anti-stiction monolayer for MEMS: A comparison to the octadecyltrichlosilane self-assembled monolayer," *J. Microelectromech. Syst.*, vol. 10, no. 1, pp. 41–49, Mar. 2001.
[24] R. Prasad, N. MacDonald, and D. Taylor, "Micro-instrumentation for tribological measurement," in *Proc. 8th Int. Conf. Solid-State Sens. Actuators, Eurosensors IX*, 1995, pp. 52–55.
[25] N. R. Tas, C. Gui, and M. Elwenspoek, "Static friction in elastic adhesive MEMS contacts, models and experiment," in *Proc. 13th Annu. Int. Conf. Micro Electro Mech. Syst.*, 2000, pp. 193–196.
[26] E. E. Flater, A. D. Corwin, M. P. de Boer, and R. W. Carpick, "In situ wear studies of surface micromachined interfaces subject to controlled loading," *Wear*, vol. 260, no. 6, pp. 580–593, Mar. 2006.
[27] U. Beerschwinger, R. L. Reuben, and S. J. Yang, "Frictional study of micromotor bearings," *Sens. Actuators A, Phys.*, vol. 63, no. 3, pp. 229–241, Dec. 1997.
[28] Q. Chen and G. Carman, "Microscale tribology (friction) measurement and influence of crystal orientation and fabrication process," in *Proc. 13th Annu. Int. Conf. Micro Electro Mech. Syst.*, 2000, pp. 657–661.
[29] Z. Guo, Y. Meng, H. Wu, C. Su, and S. Wen, "Measurement of static and dynamic friction coefficients of sidewalls of bulk-microfabricated MEMS devices with an on-chip micro-tribotester," *Sens. Actuators A, Phys.*, vol. 135, no. 2, pp. 863–869, Apr. 2007.
[30] W. R. Ashurst, C. Carraro, and R. Maboudian, "Vapor phase anti-stiction coatings for MEMS," *IEEE Trans. Device Mater. Rel.*, vol. 3, no. 4, pp. 173–178, Dec. 2003.
[31] W. R. Ashurst, M. B. J. Wijesundara, C. Carraro, and R. Maboudian, "Tribological impact of SiC encapsulation of released polycrystalline silicon microstructures," *Tribol. Lett.*, vol. 17, no. 2, pp. 195–198, Aug. 2004.
[32] U. Beerschwinger, D. Mathieson, R. L. Leuben, and S. J. Yang, "A study of wear on MEMS contact morphologies," *J. Micromech. Microeng.*, vol. 4, no. 3, pp. 95–105, Sep. 1994.
[33] U. Beerschwinger, T. Albrecht, D. Mathieson, R. L. Reuben, S. J. Yang, and M. Taghizadeh, "Wear at microscopic scales and light loads for MEMS applications," *Wear*, vol. 181–183, no. 1, pp. 426–435, Feb. 1995.

[34] B. Bhushan and X. Li, "Micromechanical and tribological characterization of doped single-crystal silicon and polysilicon films for microelectromechanical systems devices," *J. Mater. Res.*, vol. 12, no. 1, pp. 54–63, Jan. 1997.
[35] B. Bhushan and V. N. Koinkar, "Microtribological studies of doped single-crystal silicon and polysilicon films for MEMS devices," *Sens. Actuators A, Phys.*, vol. 57, no. 2, pp. 91–102, Nov. 1996.
[36] S. H. Kim, D. B. Asay, and M. T. Dugger, "Nanotribology and MEMS," *Nano Today*, vol. 2, no. 5, pp. 22–29, Oct. 2007.
[37] D. M. Tanner, W. M. Miller, W. P. Eaton, L. W. Irwin, K. A. Peterson, M. T. Dugger, D. C. Senft, N. F. Smith, P. Tangyunyong, and S. L. Miller, "The effect of frequency on the lifetime of a surface micromachined microengine driving a load," in *Proc. Int. Rel. Phys. Symp.*, 1998, pp. 26–35.
[38] D. M. Tanner, J. A. Walraven, L. W. Irwin, M. T. Dugger, N. F. Smith, W. P. Eaton, W. M. Miller, and S. L. Miller, "The effect of humidity on the reliability of a surface micromachined microengine," in *Proc. IEEE Int. Rel. Phys. Symp.*, 1999, pp. 189–197.
[39] S. T. Patton, W. D. Cowan, and J. S. Zabinski, "Performance and reliability of a new MEMS electrostatic output motor," in *Proc. IEEE 37th Annu. Int. Rel. Phys. Symp.*, 1999, pp. 189–197.
[40] S. T. Patton, W. D. Cowan, K. C. Eapen, and J. S. Zabinski, "Effect of surface chemistry on the tribological performance of a MEMS electrostatic lateral output motor," *Tribol. Lett.*, vol. 9, no. 3/4, pp. 199–209, Jan. 2001.
[41] S. T. Patton and J. S. Zabinski, "Failure mechanisms of a MEMS actuator in very high vacuum," *Tribol. Int.*, vol. 35, no. 6, pp. 373–379, Jun. 2002.
[42] D. H. Alsem, E. A. Stach, M. T. Dugger, M. Enachescu, and R. O. Ritchie, "An electron microscopy study of wear in polysilicon microelectromechanical systems in ambient air," *Thin Solid Films*, vol. 515, no. 6, pp. 3259–3266, Feb. 2007.
[43] D. C. Senft and M. T. Dugger, "Friction and wear in surface micromachined tribological test devices," in *Proc. SPIE—Micromachined Devices and Components III*, Bellingham, WA, 1997, vol. 3224, pp. 31–38.
[44] J. J. Sniegowski and E. J. Garcia, "Microfabricated actuators and their application to optics," in *Proc. SPIE—Miniaturized Systems With Micro-Optics and Micromechanics*, 1995, vol. 2383, pp. 46–64.
[45] W. C. Tang, M. G. Lim, and R. T. Howe, "Electrostatic comb drive levitation and control method," *J. Microelectromech. Syst.*, vol. 1, no. 4, pp. 170–178, Dec. 1992.
[46] L. A. Giannuzzi and F. A. Stevie, *Introduction to Focused Ion Beams: Instrumentation, Theory, Techniques and Practice*. New York: Springer-Verlag, 2004.
[47] J. F. Archard, "Contact and rubbing of flat surfaces," *J. Appl. Phys.*, vol. 24, no. 8, p. 981, Aug. 1953.
[48] J. F. Archard, "Single contacts and multiple encounters," *J. Appl. Phys.*, vol. 32, no. 8, p. 1420, Aug. 1961.
[49] B. L. Boyce, J. M. Grazier, T. E. Buchheit, and M. J. Shaw, "Strength distributions in polycrystalline silicon MEMS," *J. Microelectromech. Syst.*, vol. 16, no. 2, pp. 179–190, Apr. 2006.
[50] J. M. Fitz-Gerald, P. D. Rack, T. A. Trottier, M. Ollinger, S. J. Pennycook, H. Gao, and R. K. Singh, "Synthesis of spherical luminescent particulate coatings," *J. Appl. Phys.*, vol. 86, no. 3, p. 1759, Aug. 1999.
[51] B. Haberl, J. E. Bradby, M. V. Swain, J. S. Williams, and P. Munroe, "Phase transformations induced in relaxed amorphous silicon by indentation at room temperature," *Appl. Phys. Lett.*, vol. 85, no. 23, p. 5559, Dec. 2004.
[52] D. H. Alsem, B. L. Boyce, E. A. Stach, and R. O. Ritchie, "Effect of post-release sidewall morphology on the fracture and fatigue properties of polycrystalline silicon structural films," *Sens. Actuators A, Phys.*, 2008. in press. doi:10.1016/j.sna.2008.05.027.
[53] U. Srinivasan, J. D. Foster, U. Habib, R. T. Howe, R. Maboudian, D. C. Senft, and M. T. Dugger, "Lubrication of polysilicon micromechanisms with self-assembled monolayers," in *Proc. Solid-State Sens. Actuator Workshop*, 1998, pp. 156–161.
[54] N. P. Suh and H. C. Sin, "The genesis of friction," *Wear*, vol. 69, no. 1, pp. 91–114, Jun. 1981.
[55] N. P. Suh, *Tribophysics*. Englewood Cliffs, NJ: Prentice-Hall, 1986.
[56] U. Srinivasan, M. R. Houston, R. T. Howe, and R. Maboudian, "Alkyltrichlorosilane-based self-assembled monolayer films for stiction reduction in silicon micromachines," *J. Microelectromech. Syst.*, vol. 7, no. 2, p. 252, Jun. 1998.
[57] M. N. Gardos, "Tribological behavior of polycrystalline and single-crystal silicon," *Tribol. Lett.*, vol. 2, no. 4, pp. 355–373, Dec. 1996.
[58] M. N. Gardos, "Advantages and limitations of silicon as a bearing material for MEMS applications," in *Tribology Issues and Opportunities in MEMS*, B. Bhushan, Ed. Dordrecht, The Netherlands: Kluwer, 1998, p. 341.
[59] K. Sumino, "Deformation behavior of silicon," *Metall. Mater. Trans. A*, vol. 30, no. 6, p. 1465, Jun. 1999.
[60] A. M. Minor, E. T. Lilleodden, M. Jin, E. A. Stach, D. C. Chrzan, and J. W. Morris, Jr., "Room temperature dislocation plasticity in silicon," *Philos. Mag. A, Phys. Condens. Matter Defects Mech. Prop.*, vol. 85, no. 2, pp. 323–330, Jan. 2005.

Daan Hein Alsem received the M.S. degree in applied physics from the University of Groningen, Groningen, The Netherlands, in 2002, and the Ph.D. degree in materials science and engineering from the University of California, Berkeley, in 2006.

He is currently a Postdoctoral Fellow with the Materials Sciences Division, National Center for Electron Microscopy, Lawrence Berkeley National Laboratory, Berkeley. His primary research interests are mechanical behavior of thin films, nanomaterials, and novel structural materials, emphasizing the application of (*in situ*) analytical electron beam characterization.

Michael T. Dugger received the Ph.D. degree in materials science and engineering from Northwestern University, Evanston, IL, in 1990.

He is currently a Distinguished Member of the Technical Staff with Sandia National Laboratories, Albuquerque, NM, where he conducts a wide range of fundamental to applied research in tribology. Research topics include friction and wear in microelectromechanical systems, vapor phase lubrication, friction and wear in hard coatings, aging and performance of solid lubricants, particle generation due to wear, and the relationship between mechanical and electrical behavior of electrical contacts.

Eric A. Stach received the B.S.M.E. degree from Duke University, Durham, NC, in 1992, the M.S.M.S.E. degree from the University of Washington, Seattle, in 1994, and the Ph.D. degree from the University of Virginia, Charlottesville, in 1998.

He is an Associate Professor of materials engineering with Purdue University, West Lafayette, IN, and directs Purdue's Electron Microscopy Consortium. Prior to his appointment to Purdue, he was Principal Investigator and Program Leader within the Materials Science Division and the National Center for Electron Microscopy, Lawrence Berkeley National Laboratory. His research focuses on the development and application of advanced electron microscopy techniques for the real-time observation of nanostructured crystal growth and nanomaterials reliability.

Robert O. Ritchie received the B.A. degree in physics and metallurgy, and the M.A., Ph.D., and Sc.D. degrees in materials science from Cambridge University, Cambridge, U.K., in 1969, 1973, 1973, and 1990, respectively.

He is currently the H.T. and Jessie Chua Distinguished Professor of Engineering and the Chair of the Materials Science and Engineering Department, University of California, Berkeley, and Faculty Senior Scientist with the Materials Sciences Division, Lawrence Berkeley National Laboratory, Berkeley. His primary research interest is the mechanical behavior of engineering and biological materials.

Dr. Ritchie is a member of the National Academy of Engineering and the U.K. Royal Academy of Engineering.